Available online at www.sciencedirect.com
SCIENCE DIRECT®
Journal of Solid State Chemistry 172 (2003) 243–251
JOURNAL OF SOLID STATE CHEMISTRY
http://elsevier.com/locate/jssc

Using CBED and crystallographic image processing to evidence a structural distortion in a new family of ionic conductor $Sr_{1-x}La_{1+x}Al_{1-x}Mg_xO_4$ ($0 \leqslant x \leqslant 0.7$)

A. Magrez,[a] J.P. Morniroli,[b] M.T. Caldes,[a,*] A.M. Marie,[a] O. Joubert,[a] and L. Brohan[a]

[a] *Laboratoire de Chimie des Solides, Institut des Matériaux Jean Rouxel, Université de Nantes, UMR 6502, 2 rue de la Houssinière BP 32229, 44322 Nantes, Cedex 3, France*

[b] *Laboratoire de Métallurgie Physique et Génie des Matériaux, UMR CNRS 8517, USTL, 59655 Villeneuve d'Ascq, France*

Received 11 September 2002; received in revised form 17 December 2002; accepted 18 December 2002

Abstract

A previous study by Raman scattering of the $Sr_{1-x}La_{1+x}Al_{1-x}Mg_xO_4$ solid solution evidenced a distortion from ideal K_2NiF_4 structure. X-ray powder diffraction and selected area electron diffraction studies were carried out and no lowering of symmetry was observed. All the reflections could be indexed in the space group $I4/mmm$ with $a = b = 0.38$ nm and $c = 1.27$ nm. A coupled study by convergent beam electron diffraction and crystallographic image processing was performed. These techniques have been used to determine a crystal distortion due to small atom displacements from mirrors or axes, which lower the structure symmetry. The *mm*2 point group symmetry was determined. A microdiffraction study leads to the *Imm*2 space group. This orthorhombic distortion allows a better understanding of the ionic conductivity behavior of these compounds.

Keywords: $Sr_{1-x}La_{1+x}Al_{1-x}Mg_xO_4$ solid solution; K_2NiF_4-type structure; Convergent beam electron diffraction (CBED); Crystallographic image processing (CIP)

1. Introduction

Ruddlesden–Popper phases [1,2] with nominal composition $M_2[A_{n-1}B_nO_{3n+1}]$ have attracted much attention for a few decades. Depending on their composition, these compounds show several interesting physical properties.

Recently, Magrez et al. [3,4] have reported the synthesis and the structural characterization of the solid solution $Sr_{1-x}La_{1+x}Al_{1-x}Mg_xO_4$ ($0 \leqslant x \leqslant 0.7$), which exhibits a promising ionic conductivity behavior [5]. The crystal structure of these phases is related to the two-dimensional (2D) K_2NiF_4-type structure, which derives from an ordering of the B-sites vacancies in the ABO_3 perovskite structure. This structural model is normally described in the tetragonal $I4/mmm$ space group as an intergrowth of one perovskite layer (Al/MgO_2) between two rock-salt (Sr, LaO) slabs (Fig. 1).

The stability of such structure is controlled by the perovskite-layer/rock-salt layer mismatch, which is usually designed by the Goldschmidt tolerance factor (t).

For the solid solution $Sr_{1-x}La_{1+x}Al_{1-x}Mg_xO_4$ ($0 \leqslant x \leqslant 0.7$), this factor decreases with x value, from 0.973 ($x = 0$) to 0.901 ($x = 0.7$), indicating an increase of the internal stresses. In order to relieve the interlayer strains, atoms could be displaced from their ideal rock-salt sites and/or perovskite sites, leading to a distorted structure. In fact, a previous study by Raman scattering and FTIR absorption reveals the existence of additional bands that could not be assigned in the ideal $I4/mmm$ space group [3]. This feature indicates a distortion of the structure. However, a lowering of crystal symmetry has not been evidenced from X-ray diffraction on single crystal [6]. This result seems to indicate that the phenomenon, which is responsible of the structural distortion, exhibits a short coherence length or mainly concerns light atoms.

*Corresponding author. Fax: +33-2-40-37-39-95.
E-mail address: caldes@cnrs-imm.fr (M.T. Caldes).

0022-4596/03/$ - see front matter © 2003 Elsevier Science (USA). All rights reserved.
doi:10.1016/S0022-4596(03)00049-5

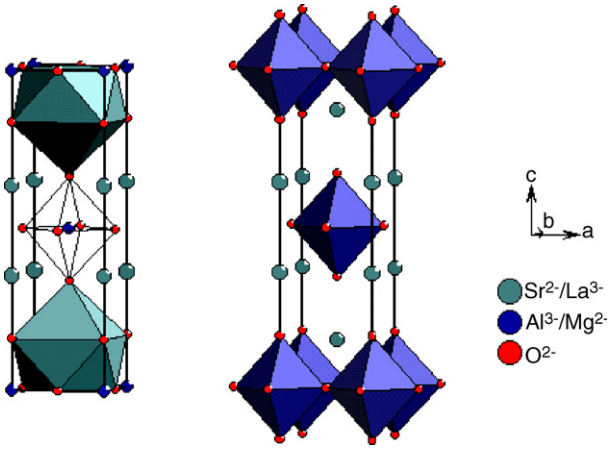

Fig. 1. Ideal K_2NiF_4 structure of the $Sr_{1-x}La_{1+x}Al_{1-x}Mg_xO_4$ ($0 \leqslant x \leqslant 0.7$) solid solution. The arrangement between the two building blocks is shown. Al^{3+}/Mg^{2+} and Sr^{2+}/La^{3+} cations are, respectively, six- and nine-fold coordinated.

Compared to selected-area electron diffraction (SAED), giving an average information of the structure, convergent beam electron diffraction (CBED) and crystallographic image processing (CIP) can be advantageously used to investigate the local symmetry of the crystal structure.

CBED has been used to obtain some structural information from a reduced region of the sample. Actually, the main advantage of CBED technique, beyond the reach of other diffraction methods, is that the information comes from nanometer specimen areas. Moreover, CBED is a powerful tool to determine the space group since direct observation of crystal symmetry can be carried out through strong dynamical-diffraction effect. Finally, since electrons interact with electrostatic potential distribution, electron diffraction can be helpfully used to solve structural problems concerning light atoms.

The symmetry of the crystal projection can also be determined from HREM images. The structure-factor phase information, which is lost during electron diffraction experiments, is present in HREM images. So, from the Fourier transform (FT) of image, the phase information is collected in order to determine the symmetry, since phase relations and restrictions are different for different symmetries.

In this work, CBED and CIP techniques have been used to evidence a nanostructural distortion in the solid solution $Sr_{1-x}La_{1+x}Al_{1-x}Mg_xO_4$ ($0 \leqslant x \leqslant 0.7$)

2. Experimental procedures

Synthesis of the $Sr_{1-x}La_{1+x}Al_{1-x}Mg_xO_4$ ($0 \leqslant x \leqslant 0.7$) compounds was achieved by the nitrate polyacrilamide gel process [4,7]. A well-crystallized single-phase product was obtained for each composition after a thermal treatment at 1400°C for 12 h.

The X-ray powder diffraction (XRPD) patterns were collected at room temperature in Debye–Scherrer geometry using an INEL position-sensitive detector with a monochromatized Cu$K\alpha_1$ radiation. A thin and very homogeneous layer of powder was put on the external side of a thin Lindeman capillary whose surface was made sticky by means of vacuum grease to prevent high-absorption coefficient of the samples. Structure refinements were carried out by the Rietveld method using FULLPROF software [8].

Samples for SAED studies were gently ground in ethanol. The microcrystals were deposited on a holed carbon film supported by a copper grid. Samples for CBED studies were laminate after mixing with 15 μm aluminum powder, in order to obtain about 20 μm thick. A 3 mm diameter disc was cut from the foil. The final thinning of the disk was performed using an argon ion-beam thinning device. The SAED and CBED studies were completed on a Philips CM30 transmission electron microscope operating at 300 kV. The HREM study was carried out with a Hitachi H9000NAR electron microscope operating at 300 kV with a Scherzer resolution of 1.8 Å. HREM images were digitized using a Nikon Multi-format LS-4500AF film scanner at 1500 dpi for preserving the resolution of the image. CIP was achieved using the CRISP software [9,10]. All the electron microscopy studies have been carried out at room temperature.

3. Results

The structure of the solid solution compounds were refined from XRPD pattern by the Rietveld method, using as starting model that was proposed by Shannon et al. [6] for $SrLaAlO_4$. The structure is considered as an ideal K_2NiF_4, described in the $I4/mmm$ tetragonal space group. The results of the final refinement for each compound are reported in Table 1.

Although reliability factors are correct, the isotropic atomic displacement parameters (ADPs) for oxygen atoms are slightly high. This feature firstly expresses that oxygen atoms are bonded to cations with different ionic radii, statistically distributed over two different sites: Sr/La ($r_{Sr^{2+}} = 1.31$ Å, $r_{La^{3+}} = 1.216$ Å) and Al/Mg ($r_{Al^{3+}} = 0.535$ Å, $r_{Mg^{2+}} = 0.720$ Å) [11]. Further, the abnormal ADPs observed could also be due to a local distortion and/or a tilt of the octahedrons of the structure, which should lead to a lowering of the space group symmetry. This distortion, claimed by a previous Raman scattering study, was not evidenced by XRPD due to the absence of metrical distortion ($a = b$). Therefore, an electron diffraction study was performed

Table 1
Atomic positions, thermal and reliability factors obtained from the Rietveld refinement, in the $I4/mmm$ space group, of the XRPD patterns of the $Sr_{1-x}La_{1+x}Al_{1-x}Mg_xO_4$ ($0 \leqslant x \leqslant 0.7$) samples

$I4/mmm$	Refined parameters	$x=0$	$x=0.1$	$x=0.2$	$x=0.3$	$x=0.4$	$x=0.5$	$x=0.6$	$x=0.7$
Lattice parameters (Å)	a	3.7544(2)	3.7688(1)	3.7825(2)	3.7913(2)	3.8042(1)	3.8163(1)	3.8301(1)	3.8443(1)
	c	12.6494(4)	12.6679(3)	12.6750(7)	12.6791(5)	12.6854(3)	12.6839(3)	12.6772(3)	12.6721(3)
Sr/La (0,0,z)	z	0.3589(2)	0.3594(2)	0.36033(5)	0.36033(5)	0.3608(2)	0.3610(2)	0.3616(2)	0.3617(7)
	B_{iso} (Å^2)	0.47(7)	0.14(6)	0.84(4)	0.91(4)	0.77(6)	0.94(6)	0.91(7)	0.87(6)
Al/Mg (0,0,0)	B_{iso} (Å^2)	0.45(8)	0.21(7)	0.71(3)	0.83(9)	0.67(7)	0.76(3)	1.18(3)	1.04(3)
O(1) (0,$\frac{1}{2}$,0)	B_{iso} (Å^2)	0.5(1)	0.7(1)	1.3(2)	1.6(4)	0.85(3)	1.1(3)	1.4(4)	0.78(3)
O(2) (0,0,z)	z	0.1627(9)	0.1655(9)	0.1664(5)	0.1672(5)	0.1694(41)	0.1713(5)	0.1711(5)	0.1740(54)
	B_{iso} (Å^2)	0.6(2)	0.7(2)	1.0(2)	0.9(2)	1.0(4)	1.5(5)	1.4(3)	1.43(6)
Reliabity factors	R_{Bragg}	2.72	2.41	2.67	2.30	2.84	2.15	1.93	2.04
	R_p	9.71	9.51	14.0	12.6	9.67	9.41	8.50	11.9
	R_{wp}	8.75	8.08	10.2	9.02	7.56	7.06	6.62	8.75

on these compounds, in order to further investigate their structure.

3.1. SAED and CBED studies

A SAED study was performed in order to reconstruct the three-dimensional (3D) reciprocal lattice. Fig. 2 shows [001], [010], [1−11] and [110] zone axis patterns from $Sr_{0.8}La_{1.2}Al_{0.8}Mg_{0.2}O_4$ ($x=0.2$), where only the zero-order Laue zone can be observed. All the diffracted spots could be indexed assuming a tetragonal lattice with $a, b = 0.378$ nm and $c = 1.268$ nm. The extinction conditions for all reflections $h\,k\,l$ were $h+k+l=2n$ indicating a body-centered (I) Bravais lattice. In addition, only the $h\,k\,0$ and $0\,k\,l$ reflections where $h+k=2n$ and $k+l=2n$ were observed, and for every $h\,0\,0$ and $0\,0\,l$ reflections h and l were always odd. These extinction rules, observed for all the solid solution range, are in agreement with the usual $I4/mmm$ tetragonal space group proposed by XRPD. Since any extra spots related to a lowering of the crystal symmetry was observed in the SAED patterns, a CBED study was carried out. The size probe used for this study was 52 nm, and patterns for $x=0.2$ are presented as representative for the complete solid solution.

Table 2 gives the diffraction groups and the corresponding 2D and 3D whole pattern (WP) symmetries which should be observed on the [001] and [100] zone axes patterns (ZAPs), for the $4/mmm$ point group as deduced from Ref. [12]. The WP taken along the [001] zone axis is given in Fig. 3a. Many Kikuchi lines are visible as well as some very weak FOLZ reflections, which form a ring. This WP displays two sets of perpendicular mirrors (m_1, m_2) and (m_3, m_4) located at 45° from each other. Thus, its symmetry is $4mm$. Due to the very weak intensity of the FOLZ reflections, this symmetry is mainly 2D.

To surely identify the 3D symmetry of this pattern, the crystal was tilted along the (m_1, m_2) and (m_3, m_4) mirrors until FOLZ and high-order Laue zone (HOLZ) reflections become visible enough. Tilt experiments along the m_1 and m_2 mirrors (Figs. 3b and c) clearly show that the HOLZ reflections are perfectly symmetrical with respect to these mirrors indicating that the m_1 and m_2 are indeed 3D mirrors. Tilt experiments along the other two m_3 and m_4 mirrors (Fig. 3d) reveal some differences between the intensity of symmetrically disposed reflections on each side of these mirrors. Thus, the others m_3 and m_4 mirrors are only 2D mirrors. It should be noted that the disappearance of a mirror plane can also be due to the existence of some structural defects. However, neither dislocations nor intergrowth defects were observed in the image of the area explored by CBED. Moreover, the existence of this kind of defects should strongly modify the CBED pattern appearance. Since we were not able to evidence the m_3 and m_4 mirrors after several experiments, we conclude that the WP 3D symmetry must be $2mm$.

This WP symmetry is not compatible with the $4mm1_R$ diffraction group. As indicated in Table 2, it could only be in agreement with the 4_Rmm_R, $2mm1_R$ and $2mm$ diffraction groups which would be observed on [001]

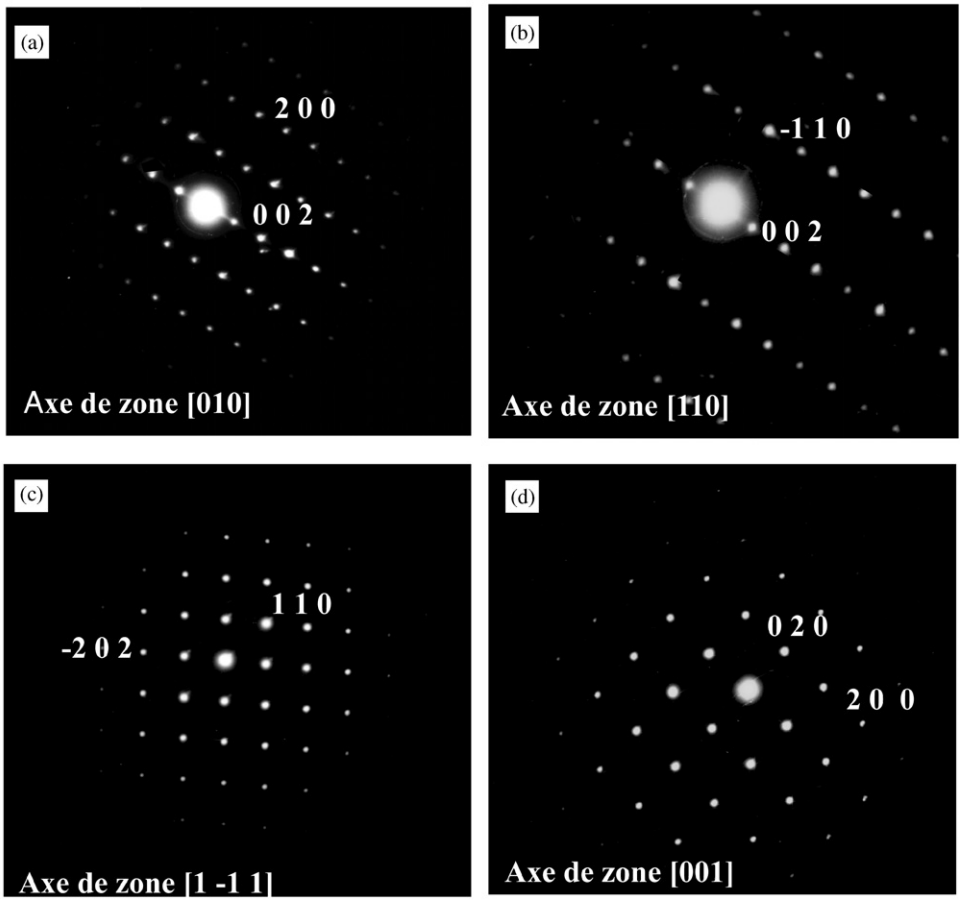

Fig. 2. SAED patterns of the $Sr_{0.8}La_{1.2}Al_{0.8}Mg_{0.2}O_4$ ($x = 0.2$): (a) [010], (b) [110], (c) [1−11], and (d) [001] zone axes.

Table 2
2D and 3D symmetries of whole patterns for the considered point groups in the CBED study

(12)	[001]	[100]
$4/mmm$	$4mm1_R$	$2mm1_R$
2D	$4mm$	$2mm$
3D	$4mm$	$2mm$
$-42m$	4_Rmm_R	$2m_Rm_R$
2D	$4mm$	$2mm$
3D	$2mm$	2
mmm	$2mm1_R$	$2mm1_R$
2D	$2mm$	$2mm$
3D	$2mm$	$2mm$
$mm2$	$2mm$	$m1_R$
2D	$2mm$	m
3D	$2mm$	m

zone axis patterns with crystals belonging to the $-42m$, mmm and $mm2$ point groups.

Table 2 also indicates that these three diffraction groups 4_Rmm_R, $2mm1_R$ and $2mm$ can be distinguished from observations of the [100] ZAP.

The [100] ZAP is shown in Fig. 4a. Just like the previous [001] pattern, many Kikuchi lines are visible and the FOLZ ring reflections are very weak. Two m_1 and m_2 mirrors are identified giving $2mm$ WP 2D symmetry. Tilt experiments along the m_1 and m_2 mirrors indicate that only the m_1 mirror is a 3D one. Therefore, the 3D WP symmetry is m.

According to these results, the structure must be described in an orthorhombic space group belonging to the $mm2$ point group, with the two-fold axis oriented along the stacking direction c.

3.2. Crystallographic image processing study

As mentioned before, the symmetry of the crystal projection can also be determined from HREM images using CIP method. The structure-factor phase information, which is lost during electron diffraction experiments, is preserved on HREM images. If the crystal is thin enough to validate the weak-phase object approximation and if the images are taken at Scherzer defocus, HREM images represent directly the projected potential and the FT of the image is proportional to the crystal structure factor. So, the amplitudes of the diffraction

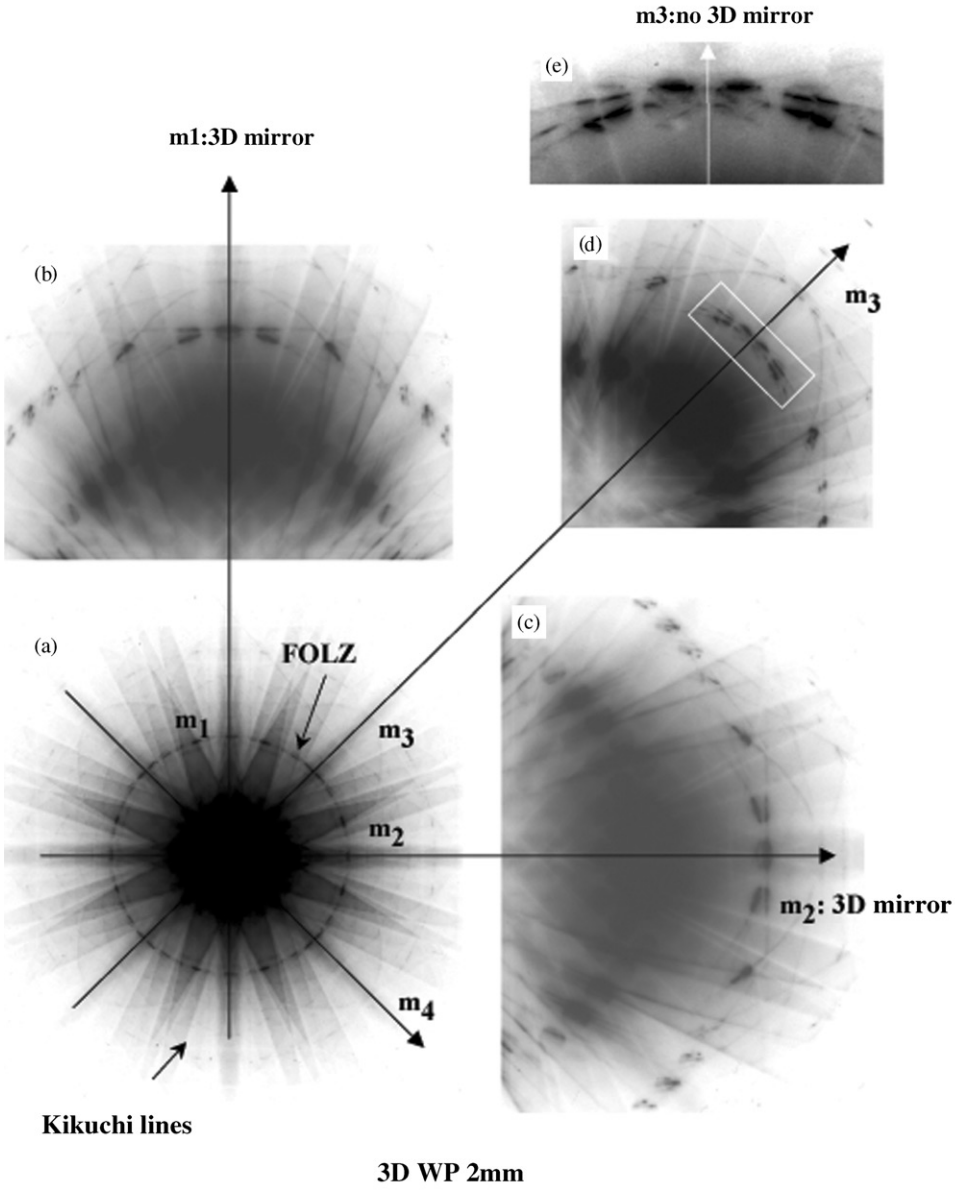

Fig. 3. (a) [001] zone axis WP of the $Sr_{0.8}La_{1.2}Al_{0.8}Mg_{0.2}O_4$ ($x = 0.2$), (b) diffraction pattern after tilting the specimen along the m_1 mirror, (c) diffraction pattern after tilting the specimen along the m_2 mirror, (d) diffraction pattern after tilting the specimen along the m_3 mirror, and (e) zoom of a part of the FOLZ from the image after tilting along m_3.

spots in the FT are proportional to those of the crystal structure factors whereas phases differ by 180° from those of the structure factors. Therefore, from the FT of image, the phase information can be collected for symmetry determination, since phase relations and restrictions are different for different symmetry [10].

In order to determine if a deviation from tetragonal symmetry occurs in the solid solution $Sr_{1-x}La_{1+x}Al_{1-x}Mg_xO_4$ ($0 \leqslant x \leqslant 0.7$), the 2D symmetry of the HREM images of $Sr_{0.8}La_{1.2}Al_{0.8}Mg_{0.2}O_4$ ($x = 0.2$) was determined by CIP.

In Fig. 5, [100] HREM image of this compound taken at Scherzer defocus (−50 nm) is presented. Using atomic position refined from XRPD pattern, a simulated image was calculated and is presented as an inset in Fig. 5. For this defocus value, rock-salt layers are imaged as black spots while the perovskite layer exhibits a gray contrast. CRISP program was used to calculate the FFT from the observed image. A square area of 512×512 pixels corresponding to 170 Å of size probe, was selected in the thinner part of the crystal. After calculating the FT of the image, the crystal lattice is refined by selecting diffraction spots and indexing them. The symmetry of the crystal projection can be determined by using the lattice vectors and phases. In CRISP, all 2D symmetries, which are compatible with the lattice vectors, are tested. The origin, which corresponds to the lowest phase residual (ϕ_{res}), is

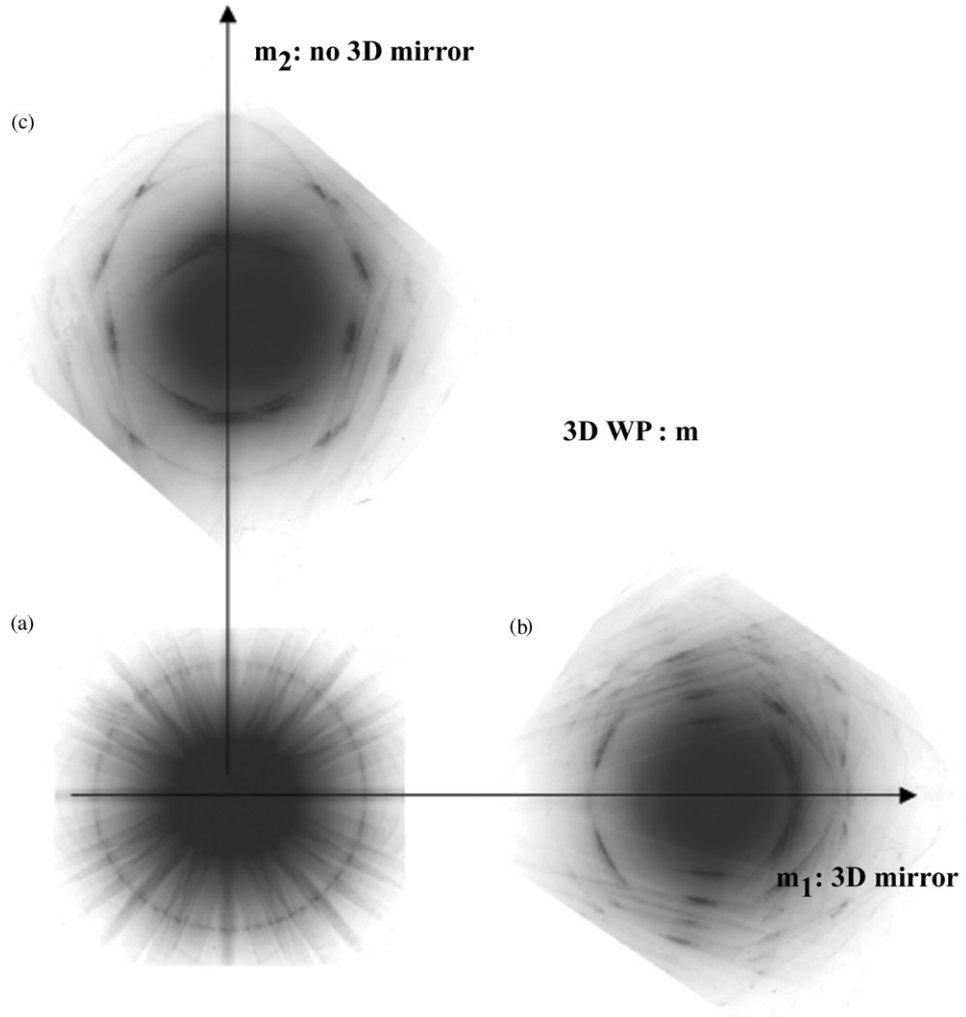

Fig. 4. (a) [100] zone axis WP of the $Sr_{0.8}La_{1.2}Al_{0.8}Mg_{0.2}O_4$ ($x = 0.2$), (b) diffraction pattern after tilting the specimen along the m_1 mirror, and (c) diffraction pattern after tilting the specimen along the m_2 mirror.

found for each symmetry. The corresponding R-value (R_{sym}) for amplitudes is also calculated and both the values of R_{sym} and ϕ_{res} are displayed. In Fig. 6, origin refinement results are given. R_{sym} and ϕ_{res} were calculated for the possible symmetries.

The great value of R_{sym} indicates that the crystal is slightly tilted specially in the thick region. It should be noted that the columns of atoms are a little smeared out into lines perpendicular to tilt axis (see Fig. 5). However, in the case of a crystal tilt, even when the amplitudes of symmetry-related reflections differ greatly, the phases are not affected for small tilts and thin crystals [10,13]. Amplitudes in HREM images are generally of low quality and not useful for symmetry determination by CIP. In fact, crystal symmetry is determined mainly from the phases. Since crystallographic structure-factor phase information is not affected by crystal tilt, the 2D symmetries *pm*, *pg* and *cm* are selected as probably crystal symmetries because they exhibit the lowest phase residual ($\approx 2^\circ$).

In Table 3, the 2D symmetries of [100] projection for the tetragonal space group $I4/mmm$ and for orthorhombic point groups *mmm*, *mm*2 and 222 are reported. From this table, we conclude that the structure of the solid solution compounds cannot be described in the $I4/mmm$ space group. In agreement with the 2D symmetry of the [100] HREM image, the lattice must be orthorhombic, and must be described in the *mm*2 point group with the two-fold axis oriented along the crystallographic *c* direction.

4. Discussion

The CBED and CIP experiments are in good agreement. The symmetry of these compounds is not tetragonal but orthorhombic. Moreover, the microdiffraction experiments performed with the same beam size as in the CBED study, to release the average phenomenon of the SAED technique, does not show different extinction rules from

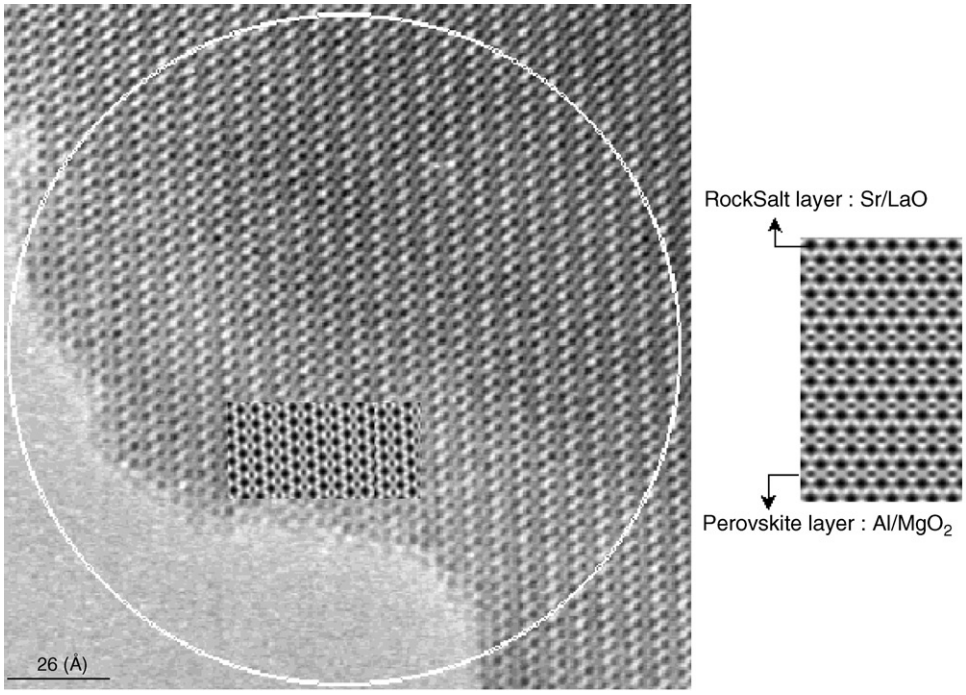

Fig. 5. [100] HREM image of the $Sr_{0.8}La_{1.2}Al_{0.8}Mg_{0.2}O_4$ ($x = 0.2$) compound. Calculated image is presented as an inset.

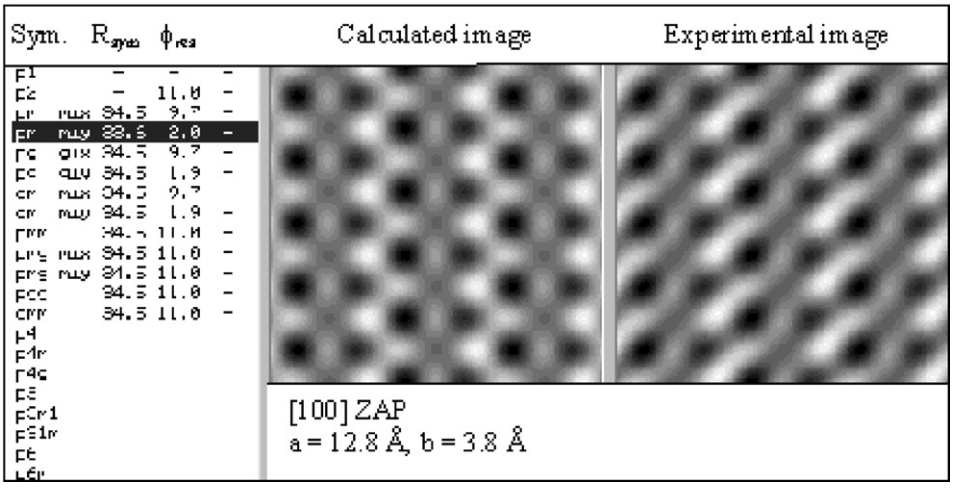

Fig. 6. Origin refinement. Deviation of amplitude and phases from each possible 2D symmetry are shown.

Table 3
2D symmetries of special projections for the tetragonal space group $I4/mmm$ and for the orthorhombic point groups: *mmm*, *mm*2 and 222

Space group	[100]
$I4/mmm$	*cmm*
Point groups	[100]
mmm	*pmm/cmm/pmgpgg*
*mm*2	*pm/cm/pg*
222	*pmm/cmm/pmgpgg*

which the SAED experiment has been observed. The structure must be described in a pseudotetragonal lattice with *Imm*2 space group and $a \sim b \sim 3.78$ Å, $c \sim 12.68$ Å.

In this non-centrosymmetric space group (see Table 4 and Fig. 7), the absence of the mirror perpendicular to the *c*-axis permits to distinguish two types of rock-salt layers which differ from the coordinates and the occupancy of the cationic site. Furthermore, along the *c*-axis, an out-of-plane displacement of the Al/Mg cation can now be described, leading to two apical interatomic distances: Al/Mg–O(21) and Al/Mg–O(22). Note that the disappearance of the four-fold axis symmetry inducing the lowering of the lattice symmetry from tetragonal to orthorhombic, is only due to the distortion of the equatorial plane: O(1)→O(11) and O(12). This structural distortion permits to reveal a particular cationic distribution Sr/La in the rocksalt layers of the

Table 4
Atomic positions of $Sr_{1-x}La_{1+x}Al_{1-x}Mg_xO_4$ ($0 \leqslant x \leqslant 0.7$) solid solution in the non-centrosymmetric *Imm*2 orthorhombic lattice

Atom	Wyck. position	x	y	z
Al/Mg	2*a*	0	0	~0
Sr/La1	2*a*	0	0	~0.64
Sr/La2	2*a*	0	0	~0.36
O11	2*b*	0	0.5	~0.5
O12	2*b*	0	0.5	~0
O21	2*a*	0	0	~0.17
O22	2*a*	0	0	~0.83

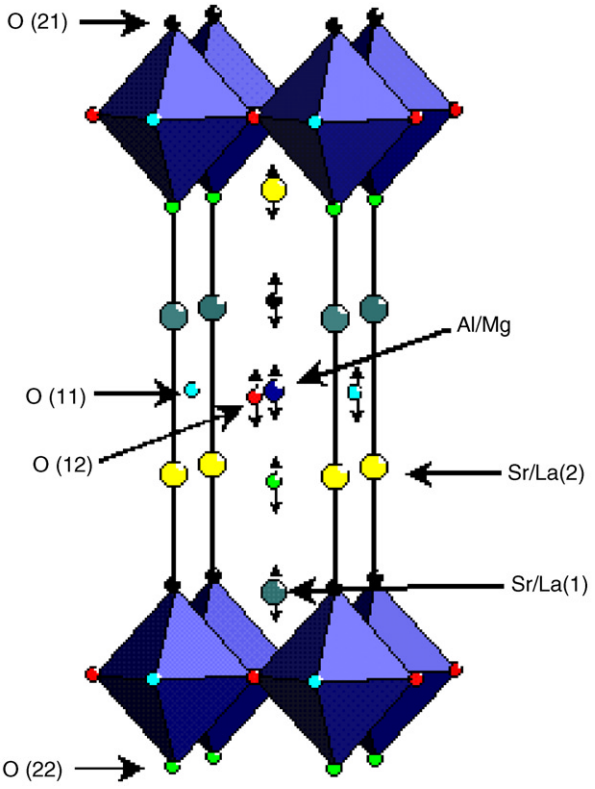

Fig. 7. Schematic model of the distorted structure. Black arrows image the atomic displacements from their ideal site.

structure. This feature could explain the dependence on strontium ratio of the activation energy of ionic conductivity in these compounds [5].

On the other hand, in order to understand the reasons why the SAED has not evidenced the symmetry lowering, two hypotheses remain possible. First of all, the crystallites are built up from nano-domains. In the case of polar structure, described in non-centrosymmetric space group, ferro-electric properties coupled with ferro-elastic properties could appear. Nevertheless, the disappearance of the mirror perpendicular to the *c*-axis leads to the existence of two ferro-elastic state oriented at 180° from each other along the *c*-axis [14,15]. In order to extract structural information from a reduced part of the crystal and avoid artifacts induced by the low coherence length, a smaller spot size than that used in SAED is necessary. In that case, CBED and CIP techniques can be useful.

The second possibility deals with the symmetry lowering is only due to the distortion of the equatorial plane of the octahedron in the perovskite layer, which concerns mainly with oxygen atoms. This kind of distortion should induce a slight non-equivalence of the $h\,k\,l$ and $k\,h\,l$ reflections. Even if, electron diffraction can be advantageously used to study structural phenomenon concerning light atoms, intensity measurements of the spots in SAED are not accurate enough to distinguish between both kinds of reflections.

Nevertheless, in CBED the dynamical-diffraction contrast within the CBED disks allows to visualize easily the crystal symmetry. The examination of the intensity distribution within individual $h\,k\,l$ reflections permits to determine unambiguously the point group. Moreover, CIP permits to obtain phase information of the structure factor, which is strongly sensitive to crystal symmetry. Therefore, a structural distortion could be easily evidenced using these techniques.

5. Conclusion

This paper deals with a local structural study of a K_2NiF_4-type structure. The structure of the $Sr_{1-x}La_{1+x}Al_{1-x}Mg_xO_4$ ($0 \leqslant x \leqslant 0.7$) solid solution has been firstly refined in the ideal $I4/mmm$ K_2NiF_4 lattice by the Rietveld method, in agreement with the SAED study. CBED and high-resolution electron microscopy techniques combined with the CIP/HREM have been used in order to evidence an orthorhombic distortion from idealized K_2NiF_4-type structure, previously inferred by Raman scattering. These techniques have allowed determining a crystal distortion due to small atom displacements.

The structural symmetry of the solid solution is described in the non-centrosymmetric *Imm*2 space group. Along the *c*-axis, the out-of-plane displacement of Al/Mg cation leads to the distortion of the octahedrons. The absence of mirror perpendicular to *c*-axis allows the existence of two rock-salt layers and the Sr/La cations are no longer statistically distributed. This orthorhombic distortion permits a better understanding of the ionic conductivity behavior of these compounds.

References

[1] S.N. Ruddlesden, P. Popper, Acta Crystallogr. 10 (1957) 538.
[2] S.N. Ruddlesden, P. Popper, Acta Crystallogr. 11 (1958) 54.

[3] A. Magrez, M. Cochet, O. Joubert, G. Louarn, M. Ganne, O. Chauvet, Chem. Mater. 13 (2002) 3893.
[4] A. Magrez, M.T. Caldes, O. Joubert, M. Ganne, Solid State Ionics 151 (2002) 365–370.
[5] A. Magrez, O. Joubert, M. Ganne, L. Brohan, to be published in Solid State Ionics.
[6] R.D. Shannon, R.A. Oswald, J.B. Parise, B.H.T. Chai, P. Byszewski, A. Pajaczkowska, R. Sobolewski, J. Solid State Chem. 98 (1992) 90.
[7] A. Douy, P. Odier, Mater. Res. Bull. 24 (1989) 1119.
[8] T. Roisnel, R. Rodriguez-Carjaval, "FULLPROF", LLB-Saclay LCSIM-Rennes, June 2001.
[9] S. Hovmöller, Ultramicroscopy 41 (1992) 121–135.
[10] X.D. Zou, Electron crystallography of inorganic structures: theory and practice, Ph.D., Stockholm University, 1995.
[11] R.D. Shannon, Acta Crystallogr. A 32 (1976) 751.
[12] D.B. Williams, C.B. Carter, Transmission Electron Microscopy, Vol. II, Plenum Press, New York, 1996, pp. 331–334.
[13] S. Hovmöller, X. Zou, Microsc. Res. Tech. 46 (1999) 147.
[14] K. Aizu, J. Phys. Soc. Jpn. 27 (1969) 3867.
[15] K. Aizu, Phys. Rev. B 2 (1970) 754.